



RESEARCH ARTICLE

Silicon Photovoltaic Cell (SPVC) Solar Panels Cause a Million Times Higher Global Warming in Comparison to the Equivalent CO₂ Gas – Experimental Evidence

Ibram Ganesh*

Centre of Excellence for Artificial Photosynthesis, International Advanced Research Centre for Powder Metallurgy and New Materials (ARCI), Balapur Post, Hyderabad – 500 005, Telangana, India

ARTICLE INFO**ABSTRACT**

Received: Aug 21, 2024

Accepted: Oct 7, 2024

Keywords

Silicon photovoltaic cells

γ- Butyrolactone

Photothermal effect
dichloromethane

Global warming

***Corresponding Author**ibranganesh@arci.res.in
dribranganesh@gmail.com

In this investigation, a systematic study was undertaken to measure the heat generating properties (i.e., photothermal effect) of commercially available multi-crystalline silicon photovoltaic (SPV) cells along with the electricity generating abilities. For this purpose, a device was designed and fabricated with two top and bottom chambers separated by thin and highly thermal conducting metal sheet such as 0.2 mm or 1.1 mm copper sheet. For this device fabrication, 21 numbers of commercially available SPV cells were used. In order to capture the complete heat generated by the SPV cells, they were fully immersed in an electrochemically and thermally quite stable organic solvent, δ-butyrolactone, and exposed to the sunlight when its power density was about 80 mW/cm², and the room temperature was 28°C to 34°C. It was found that the 21 numbers of SPV cells along with about 2 litre δ-butyrolactone upon exposure to sunlight with about 80 mW/cm² for about 2 hours during a mid-day time, the generation of about 46°C by these materials was noted. When this heat energy was captured with a low-boiling point dichloromethane (DCM) working fluid, and sent to rotate the crank-shaft of a laboratory model commercially available reciprocally moved steam engine attached with a custom made electric generator, exhibited the generation of AC electricity with >16 V. These results are presented and discussed in this article.

INTRODUCTION

It is a known fact that the carbon dioxide (CO₂) gas generated while burning the fossil fuels (crude oil, coal, natural gas, diesel, gasoline (i.e., petrol), LPG gas, LNG gas, CNG gas, etc.) to meet the energy needs of the society is causing a lot of global warming, climate change and the social cost of carbon (1-16). Today, the social cost of carbon for one ton CO₂ gas released in the atmosphere is about 2000 US\$ (17). It is also a known fact that since the beginning of the early civilization to until the starting of the industrial revolution that took place in the year 1760 across the globe, the entire world population used to depend mainly on the biomass to meet all the energy needs, and the biomass does not add any extra CO₂ gas to the atmosphere as it is formed out of the atmospheric CO₂ gas almost at the same period. Biomass is nothing but the solar energy stored by plant leaves by using CO₂ and water as energy storing materials in the form of food materials and biomass to feed human beings and animals (18-24). The utilization of fossil fuels to meet the energy needs of the society has started from the beginning of the industrial revolution, particularly, after the invention of steam engine in the year 1769, and after the discovery of electromagnetic induction to generate electricity with alternating current (AC) in the year 1831. In fact, the usage of fossil fuel has not only increased the industrialization, economy of the world and four-fold increase of the population but also the concentration of the CO₂ gas in the atmosphere leading to a severe global warming and climate change problems today (11, 25, 26). During the past 50 years, our society has survived just because of the

readymade availability of stored solar energy in the form of fossil fuels, which is also nothing but solar energy stored by plant leaves by using the same CO₂ and H₂O has energy storing materials. Our society cannot survive even for a single day today without depending on fossil fuels to meet the energy needs of our society. Even today, more than 85% of our world/global primary energy requirement (W/GPER) is met from fossil fuels only and all the CO₂ gas generated is released into the atmosphere. In the year 2023, about 36.8 billion metric tons of CO₂ is generated by burning fossil fuels and released into atmosphere. It has been estimated that >99.99% of the CO₂ gas entered into the atmosphere after starting industrial revolution during the period from 1760 to 1840 is due to the anthropogenic activities and only <0.01% CO₂ gas concentration has been entered due to the natural geologic processes such as, volcanoes eruptions, decomposition of CaCO₃ minerals, etc.. Hence, to solve global warming and climate change problems, renewable energy resources have to be utilized to meet the energy needs of the society.

The amount of renewable energy generated in the year 2023 from sunlight, wind, biomass, tide and geothermal is less than 6% of the WPER. The main focus of our society to use renewable resources to meet the energy needs has started after occurring of the oil crisis in the year 1973. The electricity production using nuclear energy was started in the year 1956, whereas, the first utility scale solar panels were employed in the year 1982, whose usage was steeply and exponentially grown after 2010. The amount of total wind power generated in the year 2022 was about 906 GW. The total electricity generated from all renewables in the year 2023 is about 29% only out of about 25 EJ electricity utilized. In the year 2023, around 277.8 TWh electricity was generated by using all the so far installed silicon photovoltaic cell (SPVC) solar panels across the globe. This is about 4.5% of the electricity used by our society in the year 2023. In terms of GPER, it does not count for even 0.2% out of 604 EJ used in the year 2022, where 277.8 TWh is equal to one Exajoule (EJ). Among the seven different types of renewable energy resources identified so far only solar energy has the capability to supply energy that is needed by our society in the year 2050. The estimated energy capabilities of these seven renewable energy resources in the year 2050 are: biomass – 5 to 7 TW, solar – about 105 TW, wind – 2 to 4 TW, tide – 2 to 3 TW, and geothermal 3 to 6 TW, and whereas, the hydroelectricity and nuclear energy outcomes depend on nature and our efforts, respectively, where, 10,000 TWh/year is equal to 1.14 TW (11). The value of solar energy outcome arrived when the solar irradiance of 1% of the Earth's surface is considered to be converted into electricity at an efficiency of 10%. In the case of renewable energy resources, except biomass all other remaining generate electricity. The movement it is an electricity, it has to be utilized immediately. Unlike biomass, electricity cannot be preserved unless it is suitably stored in any of the chemical energy forms such as, in batteries, in cylinders, or in vessels exactly like the biomass is stored in the form of chemical energy to supply to the society round the clock (RTC) 24 hours a day without any interruption like today electricity is supplied by generating at thermal power plants by burning fossil fuels without any interruption.

Today, the SPVC solar panels available in the market generate electricity with less than 20% efficiency and heat energy with more than 30% efficiency. If a one meter by two meter wide SPVC solar panel is consider (0.5 cm × 100 cm × 200 cm), it occupies about 2 square meters area and about 10 litres volume in the atmosphere. This size SPVC solar panel generates about a million times higher global warming effect in comparison to the one exhibited by the equivalent atmospheric CO₂ gas present in that 10 litres volume with a concentration of about 421 ppm (0.0421%) and it does not absorb sunlight at all but the heat infrared waves with wavelengths centered at 15, 4.3, 2.7 and 2 μm released by earth after absorbing sunlight and warmed up. Whatever the benefits of renewable electricity generated by these SPVC solar panels is compensated by the 10% excess waste heat energy generated by them. The 10% excess heat energy generated by these SPVC solar panels is equal to about a million times higher when compared with the one generated by CO₂ gas present in the volume occupied by the SPVC solar panel as the concentration of CO₂ is just 421 ppm (0.0421%). The concentration CO₂ gas in the atmosphere is million times lower than that of the silicon present in the solar panel in that given

volume. Hence, SPVC solar panels generate a million time higher heat energy than the one generated by equivalent CO₂ gas in the atmosphere. In this case, the actual amount of CO₂ gas generated upon burning fossil fuels to get that equivalent electricity by the SPVC solar panels shall not be considered. This is due to the fact that the SPVC solar panels generate higher heat energy than that of electricity. Hence, its beneficial effect is neutralized. Furthermore, during the synthesis of silicon (Si) semiconductor used in SPVC solar panels from SiO₂ sand by following the carbothermal reduction process also generates a considerable amount of CO₂ gas (SiO₂ + C → CO₂ + Si). The molar mass of carbon is 12 grams per mole, whereas, the molar mass of CO₂ gas is 44 grams per mole. Hence, each ton carbon (C) generates four tons carbon dioxide (CO₂) while synthesizing silicon (Si) metal from silicon dioxide (SiO₂) sand. That is the reason, the SPVC solar panels cause more harm to the environment than that caused by the equivalent CO₂ gas present in the atmosphere in a given volume (27).

The various other limitations of SPVC solar panels are summarized in Table 1 (8, 11). As can be seen from this Table 1, i) the theoretical efficiency of SPVC solar panels will never exceed 30% (Shockley–Queisser limit), ii) their sunlight absorption capacity is <70%, iii) their top solar glass reflects >10% incident sunlight back into the atmosphere, iv) the bus bar silver lines printed on the top surface of SPV cells block up to 8% incident sunlight, v) they generate only electricity with direct current (DC), vi) the maximum theoretical voltage generation capability of a single SPV cell is <0.7 V, vii) the efficiency of these SPVC solar panels decreases with increasing operating temperature at a rate of 0.5 V per °C rise, viii) these solar panels create a local heat island effect (a million times higher than that caused by equivalent CO₂ gas in the atmosphere), ix) they are neither repairable nor reusable, x) these solar panels need direct irradiation of sunlight unlike plant leaves absorb light from many directions, xi) these solar panels contain toxic heavy metals like Pb in the form of interconnecting wires, xii) these solar panels get easily damaged when accidentally hit by a solid object, xiii) these SPV cells require highly involved processing steps and a lot of expensive and sophisticated equipment to manufacture, and uses highly toxic and pyrophoric starting raw materials to fabricate them, xiv) when SPVC solar panels are irradiated with 3 eV light, for example, they convert only 1.1 eV equivalent light into electricity and the remaining 1.9 eV equivalent light into heat energy only. Furthermore, under open-circuit voltage (OCV) and short-circuit current (SCC) conditions, these SPVC solar panels generate only heat energy without generation of any electricity, and xv) hence, the theoretical efficiency of SPVC solar panels in modules never exceed <25% (11). Owing to these limitations, although, the SPVC solar panels have entered market almost more than 40 years back, they could not reach each and every home across the globe despite there is a lot of pressure from IPCC (Intergovernmental Panel on Climate Change) and UNFCCC (United Nations Framework Convention on Climate Change) to avoid usage of fossil fuels to meet the energy needs of the society. On the other hand, the mobile phones within their presence in the market for less than 10 years, they have reached each and every home across the globe. If any product is really beneficial, our society never ignores it to embrace for full utilization. None of the statements made about the limitations of the SPVC solar panels in this paragraph are invented by the author of this article but every statement was taken from the literature and summarized here.

In order to investigate the heat generating capability of silicon photovoltaic (SPV) cells, a device with about one square meter area has been custom manufactured using 21 numbers commercially available SPV cells, and 2 litres of γ -butyrolactone, a non-working fluid (NWF) to capture the sunlight reaching the earth surface, and to generate the heat out of the absorbed sunlight. That *in situ* generated heat energy was captured into a 2 litres volume dichloromethane (DCM) working fluid (WF) present in a copper tube conduit (3/8th inch diameter). The resultant DCM WF pressure was directed to rotate the crankshaft of a laboratory model reciprocally moved steam engine (RMSE) that is fitted with a custom made electric generator having 1500 turns of 0.2 mm copper wire coils (two or four numbers) and 4 numbers of super strong Nd₂Fe₁₄B (50 mm length × 10 mm width × 7 mm thick) magnets. Upon exposing this device to a sunlight with a power density of ~80 mW/cm² for about two hours, a generation of 17 V electricity with alternating current (AC) was noted. The temperature measured on top

surface of the top glass of the device was found to be about 46°C when the room temperature was about 34°C. The results obtained in this investigation were presented and discussed along this article.

Experimental section

2.1. Fabrication of a device to measure the heat energy generated by silicon photovoltaic (SPV) cells out of the absorbed sunlight

A schematic diagram and a digital photograph of a device fabricated and utilized to measure the temperature rising capability of SPV cells out of the absorbed sunlight are depicted in Figs. 1 & 2, respectively. The detailed schematic AutoCAD drawings of the various components utilized in the fabrication of this device are given in Figs. S1 to S4. Various numerical numbers are given in parenthesis to designate each and every component/part involved in the fabrication of this device. This device (Figs. 1 & 2) contains two-chambers (one top and one bottom) separated by a thin highly thermal conducting metal sheet (106) such as, copper (0.2 or 1.1 mm thickness), aluminum (0.5 mm thickness), etc.. In the fabrication of this device (100), 21 numbers of SPV cells (107) were employed by fully immersing in γ -butyrolactone NWF (123) present in the top chamber, and the DCM WF (124) was employed in the bottom chamber to collect the *in situ* generated heat energy out of absorbed sunlight to rotate the crank shaft of a RMSE (200) (conversion of heat energy into the rotational mechanical energy) (Fig. S5) fitted with an electric generator (300) (that turns the rotational mechanical energy into the electricity) (Fig. S6) to generate electricity with an alternating current (AC). The generation of electricity out of the sunlight by using the fabricated device (100) is shown with a block-diagram in Fig. 3. The device (100) is expected to capture >90% of the sunlight falling on the earth surface, and to convert into the heat-energy.

In Figs. S1 & S2, the parts (101) and (112) are two-numbers of the SS-304 frames with rectangular shape having outer-outer dimensions of ~1520 mm length \times ~700 mm width welded out of ~33 mm width \times ~5 mm thick flat plate bars by using the tungsten inert gas (TIG) welding technique. Each of these two frames were made to have three equally spaced openings for light transmission using two numbers of either T shaped (Fig. 2) or just a flat SS-304 bars (113) having dimensions of ~634 mm length \times 33 mm width \times 5 mm thick that divide that single major rectangular shape frame into three small size rectangular shaped openings. The T-shaped bars (113) at the center portion of the device (100) can be seen in Fig. 2. On each SS frame, 36 numbers of 12 mm diameter (ϕ) holes (125) (Figs. S3 & S4) are given, which are used to hold all the parts of the device (100) together while forming two numbers of gas-tight top and bottom chambers with the help of M10 size studs (116) and (117) tightened using two-numbers of nuts (120) on both top and bottom sides after placing both rubber (118) as well as metal (119) washers between the frame and the nuts fitted to the studs.

In the device (100), to have two-numbers of gas tight top and bottom chambers, 3 numbers of Viton (102), (105), and (111), and one ethylene propylene diene monomer (EPDM) (109) rubber gaskets with dimensions of 15 mm width \times 1.5 mm thick were employed. The top chamber is formed between the low-iron containing fully transparent, fully toughened and one-side surface-grooved Borosil solar glass (1480 mm length \times 660 mm width \times 3.2 mm thick) sheet (110) (supplied by M/s. Gujarat Borosil Ltd., India) placed on top side, and a 0.5 mm thick Al, 1.1 mm thick or 0.2 mm thick Cu sheet (1480 mm length \times 660 mm width) (106) placed on bottom side. Since, the Cu sheet with 0.2 mm is available with only 350 mm width in Hyderabad, India, two such sheets were silver brazed together by keeping them side-by-side to form a 660 mm width and 1480 mm length sheet (sometimes one side end of the sheet can be folded with 5 mm to interlock two sheets together before subjecting them to the brazing to have hermetic leak proof joint). The four sides of this gas-tight top chamber is closed with EPDM rubber gasket (109), and to maintain the gap in between top side solar glass sheet (110) and bottom side thin metal sheet (106), 21 numbers of EPDM rubber pieces (108) (~60 mm \times 60 mm size cut into plus (+) shape with 20 mm projections) were used. The T-shaped flat plate bars used in the

construction of device (100) (Fig. 2) do not allow the swelling of the center portions of the top-chamber when the volume of the DCM WF present in the bottom chamber expands by absorbing the *in situ* generated heat energy by SPV cells (107) and γ -butyrolactone NWF together. In the top chamber, gap-maintaining pieces made of Viton rubber cannot be employed as it gets swelled when it comes into contact with γ -butyrolactone NWF (123). However, EPDM is quite compatible with the γ -butyrolactone NWF (123). The 21 numbers of EPDM pieces were joined together by using 0.5 mm diameter (ϕ) Cu wire (115) and the extended portions of this Cu wires (115) were secured by placing them in between the two SS frames ((101) and (112)) tightened with nuts and bolts (or studs). These two chambers can accommodate up to 2 to 10 liters of NW and WF.

In the top chamber, 21 numbers of multi-crystalline SPV cells (107) (15.7 cm \times 15.7 cm \times <0.25 mm) (Grade A type – P157 \times P157, power 18.0%) (supplied by M/s. Adani Solar India, Ahmedabad, Gujarat, India) interconnected with Sn-Pb (Sn60/Pb40) coated Cu (\sim 1.3 mm width \times 0.2 mm thick) (supplied by M/s. the PV connect, IDA Nacharam, Hyderabad) strip (121) were also secured tightly by placing the interconnecting Cu stripes mechanically held in between the SS frames (101) and (112). About 100 mL volume glass syringe with SS needle was employed to fill this top chamber with γ -butyrolactone NWF (123). As soon as, the top chamber is filled with γ -butyrolactone NWF (123), the glass syringe along with the needle was removed, and the tightened the tie-rods and nuts fully to seal the gap so as to not to leak any γ -butyrolactone NWF (123) from top chamber into the atmosphere.

The gas-tight bottom chamber was formed between the top-side thin Cu (or Al metal) sheet (106) and bottom-side of fully toughened soda lime glass sheet (103) (1480 mm length \times 660 mm width \times 5 mm thick; supplied by M/s. Safe Glass Store, Hyderabad, India), which was also provided with two-numbers of 12 mm diameter (ϕ) holes at two-diagonal ends to fix an SS-304 cylindrical shaped pipes (104) with dimensions of 10 cm length \times 12 mm outer diameter \times 10 mm inner diameter, and one end of the pipe was given with an inner threading to fit a needle valve so as to use it as an inlet and outlet for DCM WF (124). To form the gas tight chamber and to maintain the gap in this chamber, the rubber gasket (105) and 21 numbers of Viton rubber (122) (21 numbers of \sim 60 mm \times 60 mm size cut into plus (+) shape with 20 mm projections) were employed. This bottom chamber was filled with DCM WF (124) using SS tubes 104 fitted to the bottom glass sheet. This Viton rubber is quite compatible with the DCM WF solvent employed in this study.

In order to adiabatically seal the device (100) from its surrounding atmosphere, the top surface of the low-iron containing 3.2 mm thick Borosil solar glass (110) was covered with a 0.13 mm adhesive coated fluorinated ethylene propylene (FEP) film followed by three layers of 0.15 mm thick fully transparent polyethylene terephthalate (PET) transparent polymer sheet, and then by another 0.32 mm Borosil low-iron containing solar glass to arrest the heat loss from the top glass, and the bottom 5 mm thick soda lime glass (103) surface of the bottom chamber of the device (100) was covered with two numbers of 3 mm thick silicone rubber sheet (128) followed by 0.5 mm SS metal sheet (129) in order to minimize the heat losses to the surroundings *via convection, conduction, and radiation* processes due to the presence of temperature gradient between the device (100) and its surrounding atmosphere. These diathermanous covering material, and the silicone rubber (128) and metal (129) sheet given in bottom chamber are not shown in any of the drawings for the purpose of clarity of the inner parts of the device (100). The pipes and tubes, which make up the conduit in the device (100), and the fluid passageways between the various components of the heat generating system are connected and integrated using compression fittings so as to prevent any leakage of NWF (123) or WF (124). The global normal transmission coefficient of 3.2 mm thick Borosil solar glass sheet (110) is about 0.91. Usually, for double-side anti-reflection coated low-iron containing solar cover glass, the transmission coefficient is higher than 0.94.

Fabrication of reciprocally moved steam engine (RMSE)

A schematic drawing and a digital photograph revealing the partial details of RMSE (200) employed in this investigation to convert the *in situ* generated heat energy by the device (Fig. 2) into rotational mechanical energy is shown in Fig. S5. The WF (124) with a minimum pressure of >1.5 bar leaves the bottom chamber of the device (100) under suitable experimental conditions *via* a controlled valve into the steam chest (201) of RMSE (200) thereby moved into the main cylinder (202) *via* inlet port (207). That has caused the movement of the piston (203) in the main cylinder so as to move it reciprocally with the help of the eccentric plate (221) connected to the main cylinder piston *via* a connecting rod (218) (or joint) and axle (219) with the help of the pressure of the WF. When the eccentric plate (221) connected to the crank shaft (220) caused the rotation of another eccentric plate (223) sat on the crank shaft (220) adjacent to the eccentric plate (221) that is connected to the main cylinder piston. When this latter eccentric plate (223) was rotated, it also moved the sliding D valve cum piston rod (210) and (211) in the steam chest cum sliding D-valve chamber with the help of a connecting rod (213). The pistons (203) and (211) and the connecting rods (218) and (213) are joined with the help of two numbers of cross head bearings (204) and (212), respectively. When both the pistons (203) and (211) were reciprocally moved, they have caused the entering and exit of the WF (124) vapour *via* ports (207) and (208), respectively. The one-side dead-end of the piston (203) caused the pushing off of the WF (124) vapour out of the main cylinder *via* exhaust port(s) (207), when it got aligned with the opening ports of the center hole (208) given through the piston connected to the steam chest cum sliding D-valve chamber (209). The main cylinder was connected to the steam chest cum sliding D-valve chamber (209) as shown in Fig. S5 using silver brazing technique and this latter assembly was fixed to a stand (215), which in turn was fixed to a base plate (217) using screws (214) and (216). The crank shaft (220) and flywheel (225) are fixed to the base plate (217) using two-numbers of holders (222) with the help of screws (224).

Fabrication of electric generator

A custom made electric generator (300), whose schematic diagram shown in Fig. S6 was attached to the crankshaft (220) of the RMSE (200) (Fig. S5) to generate electricity according to the principles of *Faraday's and Lenz laws of electromagnetic induction* when the WF (124) vapour causes the movement of pistons (203) and (211) by entering *via* the steam chest port (201) of RMSE (200). The electric generator used in this study to generate electricity from sunlight had 4 numbers of rare earth neodymium ($\text{Nd}_2\text{Fe}_{14}\text{B}$) super strong magnets (50 mm length \times 10 mm width \times 7 mm thick) (301), which were firmly fixed in the four slots made on a machined nylon rod (302) (40 mm diameter (ϕ) and 50 mm length) as schematically shown in Fig. S6. At the center of this nylon rod (302), a hole of 5 mm diameter was made so that it can firmly sit on the crankshaft rod (220) of the RMSE (200). The nylon rod (302) fixed with four numbers of super strong magnets (301) was placed at center and equidistance from either four or two Cu coils (303), which are fixed to 6 mm thick transparent polypropylene (PP) sheets (304) so that the magnets (301) placed on nylon rod (302) are easily rotated with the crankshaft (220) of the RMSE (200) at center of these four or two Cu coils. The Cu coils were made by winding 1500 cycles of 0.2 mm diameter (ϕ) insulated wire on a PP piece of 3 mm thick \times 8 mm width \times 50 mm length. These four or two numbers of 1500 turns containing Cu coils are firmly fixed to the 3 mm thick plastic sheet (305) that is fixed to the base using super strong glue (quick fix solution) with the help of 6 mm thick transparent PP legs (306).

RESULTS

Effects of parameters variation on the heat generating capability of silicon photovoltaic (SPV) cells

A device (100), whose front and back views can be seen from Fig. 2 (a) & (b), respectively, was fabricated in this study as mentioned in the experimental section and was exposed to the sunlight by placing it on a metal stand at an inclination of 30° while facing the south side between 11 am and 3 pm during the sunny days of the first-half of March month of 2020, where the average power density of the sunlight was $\sim 80 \text{ mW/cm}^2$ and the average room temperature

of the surrounding atmosphere was $\sim 28^{\circ}\text{C}$. The dimensions of the device were chosen for this study based on the solar glass sheets available in the market (in Hyderabad, India) and to have the light capturing area of at least one square meter as it receives about one kWh equivalent sunlight in an hour time on a normal sunny day. This is the minimum area required to generate the desired pressure in DCP WF to rotate the armature of the electric generator fixed on the crank shaft of RMSE to produce the measurable electricity using a multimeter with the help of an electric generator. The amount of γ -butyrolactone NWF and the number of SPV cells present in the top-chamber of the device (Fig. 2 (a)) are ~ 9 litres and 21, respectively, whereas, the bottom chamber had 2 litres of DCM WF (Fig. 2 (b)). The heat-energy *in situ* generated by SPV cells and γ -butyrolactone upon exposure to the sunlight was found to transfer from the top-chamber to the bottom chamber through the 0.5 mm thick Al metal sheet (this experiment had 0.5 mm Al sheet, and some other experiments had 0.2 mm or 1.1 mm Cu sheet). The boiling of DCM WF upon exposure of the device containing 0.5 mm thick Al sheet to the sunlight can be seen from Video 1. The results obtained under various experimental conditions are summarized in Table 2. The 0.2 mm thick copper sheet possesses four times higher thermal conductivity than that of 0.5 mm thick Al sheet as the thermal conductivity of the Al is half-of-the one exhibited by the Cu metal. The beneficial effects of using 0.2 mm thick Cu sheet in this device can be seen from the results of Table 2. However, when the device was exposed to the sunlight, it got swelled considerably as can be seen from Fig. 4 (a) & (b), and within two hours of its exposure, it got swelled in such a way that it might even exploded if this exposure was continued for some more time. To avoid such an explosion, the top-solar glass surface of the device (Fig. 2 (a) & (b)) was immediately covered with a black rubber sheet completely to avoid the reaching of the sunlight to the top surface of the device. Furthermore, to avoid swelling of the chambers of device, the flat shaped SS 304 frames (Fig. 4 (a) & (b)) used as tie-rods were replaced with T-shaped ones (Fig. 2), and to avoid heat-loss through the bottom transparent soda-lime glass sheet, it was supported with two-layers of 3 mm thick EPDM rubber sheet followed by 0.5 mm thick SS sheet, and in place of 0.2 mm thick Cu sheet, a 1.1 mm thick Cu sheet was employed. When this modified device (Fig. 2) was exposed to the sunlight, within 2 hours' time, the top light transmitting solar glass got exploded completely, and both the solutions (i.e., γ -butyrolactone NWF and DCM WF) from both top and bottom chambers were come out of the device as the considerable amount of pressure generation was noted inside the device as the swelling of both top and bottom chambers and the loss of heat transfer through bottom glass was completely restricted. The high pressure *in situ* generated had severely bent the 5 mm thick SS-304 frames and 1.1 mm thick Cu sheet as can be seen from Fig. S7 (a-d). This incident can be considered as a proof of the absorbance of sunlight by the SPV cells when they were fully immersed in γ -butyrolactone and exposed to the sunlight, and generating heat-energy out of the absorbed sunlight to boil and increase the volume of DCM WF present in the bottom chamber. In this case, all the generated pressure can be attributed only to the evaporation of DCM WF as γ -butyrolactone NWF does not generate any pressure below 50°C as its boiling point is 200°C .

After the device got exploded, a Cu tube conduit (Fig. S8) fabricated out of $3/8^{\text{th}}$ diameter Cu tube was used to store the DCM WF in the bottom chamber instead of directly in the rectangular shaped bottom chamber of the device formed between Cu sheet and the glass sheet. It was found that the rectangular shaped chambers cannot withstand high pressures without undergoing any deformation (in this case swelling), and only cylindrical shaped tubes can withstand such pressures without undergoing any dimensional deformation. Probably that could be the reason behind using cylindrical shapes for the construction of all the pressure tanks and gas cylinders. In fact, the cylinder shape does not allow any deformation but rather it gets exploded when the inside pressure exceeds the withstanding capability of the construction wall of the tube/cylinder material. Since, the Cu sheet employed had a thickness of 1.1 mm, the Cu conduit tube could be easily brazed to it without allowing the formation of any pin-holes and to increase the required heat transfer from top-chamber to the bottom-chamber (i.e., from γ -butyrolactone NWF to DCM WF).

The modified device as shown in Fig. 5 (a) & (b) exhibited a voltage generation of about 16-17 V electricity with AC when exposed to sunlight for about two-hour time with the help of a RMSE, and a custom-made four magnets containing electric generator (Video 2). The 21 SPV cells present in the device actually generates only 10 V DC electricity when they are connected in series in a commercial SPVC solar panel by following the photoelectric effect. However, the same 21 SPV cells in this device generated >16 V electricity with AC even though the electric generator was not fabricated according to the standard design procedure. Furthermore, in other experiments conducted on 28th and 29th days of March 2022 using this modified device with 30 SPV cells (Fig. 5 (a) & (b)), the generation of pressure exceeding the reading capabilities of the pressure gauges (>30 bar) are noted (Fig. 6 (a) & (b)). The glowing of a 5 W LED bulb with the pressure generated by this modified device containing 30 SPV cells and with the help of a commercially procured small-size DC generator can also be seen from Figs. S9 & S10. The amount of current generated is not measured, because these experiments were aimed only to show the *proof of concept (PoC)* of heat generating capability of SPV cells, and as there is huge heat-loss associated with these devices that do not allow to measure the true temperature rising or heat generating capability of SPV cells.

In order to establish that the SPV cells and γ -butyrolactone are needed together to turn sunlight into heat-energy, the control experiments were also conducted. For this purpose, three devices with same dimensions and using similar components were fabricated. One device had both 30 SPV cells and 2 liters γ -butyrolactone in the top-chamber, the second device had only 30 SPV cells in the top-chamber, and the third device had neither SPV cells nor γ -butyrolactone in the top-chamber. These three devices had about 1.8 liters DCM WF in the bottom chambers of their copper tube conduits. These three devices were exposed to sunlight on 5th January 2022. The pressures generated in the gauges attached to the manifolds of copper conduits are plotted in Fig. 7. It can be seen that to generate the required pressures to rotate the piston of the RMSE to generate electricity, both SPV cells and γ -butyrolactone are compulsorily required, and neither only SPV cells nor the empty top-chamber generated pressures higher than 1 bar as there was a continuous leakage of the heat from the device surfaces into the atmosphere. On 25th February 2022 (i.e., on a normal sunny day), when a device (Fig. S10 (a-g)) was exposed to the sunlight and measured the temperature of its top solar glass surface by placing the tip of the thermometer on its top surface, a reading of about 47°C was noted (Video 3), which is about 14°C higher temperature than that of ambient room temperature of that day (about 32 to 34°C) at about 13:30 h. Surprisingly, during the measurement, a small wind was blown for few seconds, and immediately, a reduction of about 2°C temperature in the thermometer reading was seen from the same video (Video 3). It clearly indicates that there is a continuous loss of the *in situ* generated heat energy into the atmosphere by means of *conduction*, *convection* and *radiation* through the top glass surface due to the temperature difference between device glass surface and its surrounding atmosphere. This heat loss is the top-most obstacle to measure the true heat energy generating capacity of SPV cells. The second major obstacle is the steam engine employed in these experiments is a laboratory model device designed for engineering students' experiments purpose, which is associated with huge leakages from the piston-cylinder gaps. At present, the atmospheric weather conditions such as, ambient temperature, wind speed and its direction, humidity in the atmosphere, etc., were found to have a profound effect on the heat generating capability of the SPV cells when employed this particular device design.

The considerably high thermal conductivity of Borosil solar glass could also be one of the reasons for the higher amounts of *in situ* generated heat loss occurring through the device top surface into the atmosphere. In fact, high thermal conducting solar glass is required for SPVC solar panels and this highly thermal conducting Borosil solar glass is a must for dissipating the *in situ* generated heat energy by SPV cells as soon as possible as the efficiency of SPVC solar panels is inversely proportional to the operating ambient temperature of the cells. This is the reason for the local heat island effect normally seen wherever large number of SPVC solar panels are deployed (27). However, the device needed to measure the heat generating effect of

the SPV cells shall use glass sheet with the lowest possible thermal conductivity. In the control (i.e., blank) experiment, where, the device did not had any SPV cells or γ -butyrolactone, the temperature measured on the top the Borosil solar glass surface was found to be not much different from the one measured at ambient room temperature although certain pressure was noted in the Cu conduit containing DCM WF. These results clearly suggest that the semiconducting materials along with NWF capture more sunlight and turns it into the heat-energy. When wind was blowing, the increased heat-loss was also noted (Video 3).

The theoretical heat generating capability of SPV cells vs. experimentally determined results

The specific heat capacity (C_p) and materials weights involved in the experiment conducted as per the 2nd row of Table 2 are given in Table 3. When the top and bottom-chambers of the device (Fig. 2) were filled with about 2.3 liters of γ -butyrolactone NWF and about 2 liters of DCM WF, respectively, and then exposed to the sunlight from 11 am to 3 pm (i.e., for 4 h duration) continuously on the 13th March 2020 at ARCI, Hyderabad, Telangana, India, the amount of total sunlight that fell on the surface of the device top solar glass sheet during 4 h period was determined as mentioned below. On the experiment conducted day, the recorded room temperature at about 11 am and the average power density of the irradiated sunlight were measured to be $\sim 28^\circ\text{C}$ and $\sim 80 \text{ mW/cm}^2$, respectively.

$\Rightarrow 80 \text{ mW/cm}^2 = 800 \text{ W/m}^2 = 0.8 \text{ kW/m}^2 = 0.8 \text{ kWh/m}^2$ (for 1 hour duration); $\Rightarrow 0.8 \text{ kWh/m}^2 \times 4 \text{ hours} = 3.2 \text{ kWh}$.

The total sunlight capturing active area of the device (Fig. 2) was:

$\Rightarrow (1464 \text{ mm} \times 644 \text{ mm}; \text{ total panel rectangular area}) - (33 \text{ mm} \times 644 \text{ mm} \times 2 \text{ numbers}; \text{ it is the area covered by T-shaped bars used to divide the rectangular SS frames into three equally spaced openings})$

$\Rightarrow 9428.16 \text{ cm}^2 - 425.04 \text{ cm}^2; \Rightarrow 9003.12 \text{ cm}^2;$

$\Rightarrow 0.9003 \text{ m}^2$.

The total area of sunlight that can be captured by 21 numbers of multi-crystalline silicon (*mc-Si*) cells in the device (Fig. 2) is derived as mentioned below:

$\Rightarrow (15.7 \text{ cm} \times 15.7 \text{ cm} \times 21 \text{ numbers}) - (33 \text{ mm} \times 644 \text{ mm} \times 2 \text{ numbers}; \text{ it is the area of T-shaped bars}) - (8\% \text{ area covered by silver grid and bus-bar lines printed on the surface of SPV cells})$

$\Rightarrow 5176.29 \text{ cm}^2 - [400 \text{ cm}^2 + 414.10 \text{ cm}^2]$

$\Rightarrow 5176.29 \text{ cm}^2 - 814.10 \text{ cm}^2$

$\Rightarrow 4362.19 \text{ cm}^2$

$\Rightarrow 0.4362 \text{ m}^2$.

The packing factor is termed as the total sunlight capturing *mc-Si* cells area divided by the total active sunlight capturing area by the device (Fig. 2).

$\Rightarrow 0.4362 \text{ m}^2 / 0.9003 \text{ m}^2$

$\Rightarrow 0.4845$.

The total amount of sunlight that could be captured by the device (Fig. 2) is determined as mentioned below:

About 10% of the sunlight falling on the panel is normally reflected by the top Borosil solar glass, and if another 10% miscellaneous losses are considered, then the remaining 80% light can be captured by the device (Fig. 2). The 80% of 3.2 kWh is equal to 2.56 kWh (= 3.2 kWh \times 0.8).

Out of which, the amount of light energy to be captured at a rate of 30% by γ -butyrolactone NWF present in the area of 0.9003 m² is equal to 0.691 kWh per 0.9003 m² area in 4 h duration (= 2.56 kWh \times 0.9003 m² \times 0.3). The amount of light that is captured by SPV cells at a rate of 70% is equal to 0.7816 kWh (= 2.56 kWh \times 0.4362 m² \times 0.7). The total solar energy that could be captured by the device (Fig. 2) is equal to 1.4726 kWh (= 0.7816 kWh + 0.691 kWh).

The captured sunlight energy (i.e., 1.4726 kWh) amounts to only about 57.52% of the solar energy (i.e., 2.56 kWh) fell on the 0.9003 m² surface area of device (Fig. 2) during 4 h period. If nano-size amorphous silicon powder is employed in place of *mc-Si* cells in 0.9003 m² area with γ -butyrolactone NWF so as to appear like a liquid crystal display (LCD) screen, instead of 57.52%, the captured sunlight energy would have been 100%.

On the other hand, the amount of energy required to raise the temperature of the contents of the device (Fig. 2) by 1°C can be derived by using Eq. 2.

$$Q = C_p * m * dT \quad (2)$$

Where, the Q is the amount of energy (in kJ) required to raise the temperature (dT) of the contents having a mass of m kgs. As per the data given in Table 3, the heat capacity of the entire four major heat capturing materials (i.e., SPV cells, γ -butyrolactone NWF, Al sheet, and DCM WF) present in the device as per reaction conditions given in 2nd row of Table 2 can be derived as follows:

$$\Rightarrow 0.71 \text{ kJ/kg}^{\circ}\text{C} \times 0.2499 \text{ kg} \times 1^{\circ}\text{C} \text{ for SPV} + 0.90 \text{ kJ/kg}^{\circ}\text{C} \times 1.02 \text{ kg} \times 1^{\circ}\text{C} \text{ for Al metal sheet} + 1.642 \text{ kJ/kg}^{\circ}\text{C} \times 2.576 \text{ kg} \times 1^{\circ}\text{C} \text{ for } \gamma\text{-butyrolactone} + 1.188 \text{ kJ/kg}^{\circ}\text{C} \times 2.660 \text{ kg} \times 1^{\circ}\text{C} \text{ for DCM}$$

$$\Rightarrow 0.177429 \text{ kJ} + 0.918 \text{ kJ} + 4.2299 \text{ kJ} + 3.16008 \text{ kJ}$$

$$\Rightarrow 8.4854 \text{ kJ.}$$

The amount of heat energy (kJ) required to raise the temperature of the heat capturing materials involved in experiment conducted as per the reaction conditions given in 2nd row of Table 2 by 1°C is about 8.4854 kJ. The amount of solar energy that can be captured by both SPV cells + γ -butyrolactone NWF is about 1.4726 kWh, which is equivalent to 5297.122 kJ since 1 kJ = 0.000278 kWh. Whereas, to raise the temperature by 1°C of the heat capturing materials of the device (Fig. 2), it needs the energy about 8.4854 kJ. In that case, 5297.122 kJ (i.e., the total solar energy captured by the device (Fig. 2)) can raise the temperature of the contents by 624.26°C (= 5458.63 kJ/8.4854 kJ) if there is no heat loss to the surroundings. That means at the end of reaction conducted for about 4 h under the irradiation of sunlight at a power density of 80 mW/cm², when there was no loss of the *in situ* generated heat, then the total temperature of the contents of the device (Fig. 2) should reach a temperature of 624.26°C at a rate of heating of 2.60°C per minute (=624.26°C/240 minutes). Since, the initial temperature (i.e., room temperature) of the heat absorbing materials on the 13th day of March 2020 at ARCI, Hyderabad, Telangana, India, was about 28°C during the starting of the experiment at 11 am, to reach the boiling temperature 40°C of DCM WF, about 4.6158 min time is required (i.e., 40°C–28°C = 12°C; when the temperature of the contents is raised at the rate of 2.935°C per min (4.477 min = 12°C/2.60°C per min) if the heat transfer from γ -butyrolactone NWF present in the top-chamber through 0.5 mm thick Al metal sheet to DCM WF present in the bottom chamber is immediate. However, it took about 14 min time to start boiling of the DCM WF in the bottom chamber after exposing the device (Fig. 2) to the sunlight.

The amount of vapor pressure that can be generated out of DCM WF upon exposure to 100°C during the experiment can be derived theoretically by using the Clausius-Clapeyron equation is given in Eq. 3.

$$\ln \left(\frac{P_1}{P_2} \right) = - \frac{\Delta H_{vap}}{R} \left(\left(\frac{1}{T_1} \right) - \left(\frac{1}{T_2} \right) \right) \quad (3)$$

Where, P_1 (134 mmHg or 134 torr) is the vapour pressure of DCM WF at temperature at 0°C or 273.15 K (T_1); P_2 is the vapor pressure of the DCM WF at temperature at 100°C or 373.15 K (T_2); ΔH_{vap} is the enthalpy of vaporization of DCM WF, which is equal to about 2850 J.mol^{-1} ; and R is the universal gas constant, about $8.314 \text{ J.mol}^{-1} \cdot \text{K}^{-1}$. As the temperature gradient between the γ -butyrolactone NWF and DCM WF increases, the heat transfer from NWF to WF takes place via 0.5 thick Al or 0.2 mm thick Cu sheet.

The value of P_2 can be determined as follows:

$$\Rightarrow \ln \left(\frac{P_1}{P_2} \right) = - \frac{30855.104}{8.314} (\text{J.mol}^{-1}/\text{J.mol}^{-1} \cdot \text{K}^{-1}) \left(\left(\frac{1}{273.15} \right) - \left(\frac{1}{373.15} \right) \right) (\text{K}^{-1})$$

$$\Rightarrow \ln \left(\frac{P_1}{P_2} \right) = - 3711.210 (\text{J.mol}^{-1}/\text{J.mol}^{-1} \cdot \text{K}^{-1}) \times 0.00098110 (\text{K}^{-1})$$

$$\Rightarrow \ln \left(\frac{P_1}{P_2} \right) = -3.641; \Rightarrow \ln(P_1) - \ln(P_2) = -3.641; \Rightarrow \ln(134 \text{ mmHg}) - \ln(P_2) = -3.641;$$

$$\Rightarrow 4.897 \text{ mmHg} - \ln(P_2) = -3.641; \Rightarrow -\ln(P_2) = -3.641 - 4.897 \text{ mmHg};$$

$$\Rightarrow -\ln(P_2) = -8.5382; \Rightarrow \ln(P_2) = 8.5382; \Rightarrow P_2 = e^{8.5382} \text{ mmHg};$$

$$\Rightarrow P_2 = 5105.12 \text{ mmHg (torr)}; \Rightarrow P_2 = 5105.12/760 = 6.717 \text{ atm.}$$

To reach the boiling point 40°C of 2 liter volume DCM WF, about 4.5 min time is needed under adiabatic conditions. That means a pressure of 2.5894 atm. (or bar) reaches according to the *Clausius-Clapeyron* equation (Eq. 3). However, during experiments, as soon as the pressure in the bottom chamber of the device (Fig. 2) reached 1 bar, the WF was released to rotate the crank shaft of the RMSE that is connected with an electric generator having four super strong magnets and two Cu coils using a 6 mm outer diameter (OD) and 4 mm inner diameter steel pipe, and to reach 1 bar pressure, it took about 14 min time. It confirms that there is a considerable amount of heat loss from the device (Fig. 2) into the atmosphere, which needs to be addressed by employing proper components such as, a flat glass vacuum chamber that works like a Dewar flask wall in arresting heat loss on top of the device (Fig. 2) to transmit only sunlight into the device but no heat loss from inside of the device into the outside surrounding atmosphere, and polyurethane foam (PUF) heat insulation at the bottom of the device (Fig. 2), etc., in its construction.

DISCUSSION

It is a known fact that even a two-degree centigrade rise in the temperature is considered as a huge and quite detrimental when it is come to human body as well as to our globe. As shown in Video 3, the temperature reading in the thermometer was about 46°C when the room temperature was about 32 to 34°C (these room temperature values can be found even in the meteorological records of Telangana State Government, India). Continuous release of that much heat into the atmosphere by large scale deployed SPVC solar panels can be considered a huge negative effect on the global temperature. It is a well-documented fact in the literature that the SPVC solar panels rise local temperature, which is popularly termed as “*Local Heat Island*” effect when deployed in relatively large areas (27). Even the design of the SPVC solar panels is made in such a way that it dissipates heat as early as possible to the atmosphere by maintaining the thickness of the construction materials as minimum as possible for fast dissipation of heat generated by SPVC solar panels. In fact, to utilize the heat generated by SPVC solar panels to improve their efficiency as it is inversely proportional to the operating temperature of SPV cells, and to use it for beneficial purposes of human society the hybrid photovoltaic thermal (PV/T) solar panels were designed and tested (28-36). In these hybrid photovoltaic thermal (PV/T)

solar panel systems, a cooling liquid is circulated to collect the heat generated by SPV cells. However, in these PV/T systems, the cooling liquid does not come directly in contact with the SPV cells, whereas, in the present study, γ -butyrolactone NWF had a direct contact with the SPV cells. In the so far reported studies on PV/T systems, the stagnation, although infrequent, is a possible occurrence in forced circulated solar PV/T thermal systems (32, 37, 38), and is caused by low thermal demand (fully charged thermal storage tank), power outages (no electricity available to run the pumps) and other problems leading to a no-flow condition (plugged pipes, leaks, broken pumps, etc.). In these situations, the collector temperatures only depend on the idle heat losses and on the insolation heat dissipating capability. Consequently, stagnation temperatures sometimes reach up to 220-350°C for evacuated tube collectors, 170-210°C for flat-plate collectors with selective absorbers and 115-150°C for flat-plate collectors with non-selective absorbers (39). Although, the SPV cells can withstand temperatures up to 220°C, the EVA encapsulate loses its mechanical properties at 130-140°C and undergo delamination (39). The occurrence of such high collector temperatures can cause the accelerated ageing of temperature sensitive components leading to their eventual failure, safety hazards for humans, uncomfortable acoustic emissions due to condensation pressure shocks (measured up to a maximum pressure of 6 bar for 60% water + 40% propylene glycol solution), enhanced vulnerability to hot spots resulting from manufacturing imperfections and the vaporization of common heat carrier fluids, and their potential release into the atmosphere from the loop *via* safety valves. Owing to these problems, although the overall STE conversion efficiency of PV/T systems has been found to be a bit higher than those of pure SPVC solar panels, their usage has been very limited. Nevertheless, the components used in the fabrication of SPVC solar panels such as low iron containing top solar glass, and the EVA polymer layer ensure that maximum amount of *in situ* generated heat energy is dissipated as soon as possible, which is the reason behind the normally absorbed “*local heat island effect*” when a large number of SPVC solar panels are deployed (40). As mentioned in the introduction section, the more than 10% heat efficiency generated by SPVC solar panels than electricity generated by them is a million times higher in comparison to the heat effect generated by the equivalent CO₂ gas released into the atmosphere by burning fossil fuels to generate electricity that can be generated by SPVC solar panels. It is a known fact that the SPVC solar panels are not only deployed to generate renewable electricity (i.e., as an alternative energy vectors) but also to avoid the global warming caused by the CO₂ gas that is generated upon using of fossil fuels to meet the energy needs of the society. In fact, the net benefit of the electricity generated by SPVC solar panels is zero. This is due to the fact that they generate less than 20% electrical efficiency and more than 30% heat energy efficiency. In fact, these SPVC solar panels are generating 10% excess heat energy than they can generate the electricity. Upon irradiating the SPVC solar panels with a sunlight photon having energy equivalent to 3 eV, in that case, the light energy equivalent to 1.1 eV is converted into electricity, and light energy equivalent to the remaining 1.9 eV (=3.0 eV – 1.1eV) is converted into heat energy, which is released in the atmosphere. It is also a known fact that under OCV and SCC conditions, the SPVC solar panels generate only heat energy without any electricity. The concentration of Si semiconductor on the surface of the SPVC solar panels that is exposed to sunlight to absorb is >90%, whereas, the concentration of CO₂ gas in the atmosphere is 0.0421% (421 ppm) (that means the concentration of silicon in the solar panel is >92%, whereas, the concentration of CO₂ in the atmosphere is only 0.0421%, which is lower than a million times). Hence, obviously, the CO₂ gas in the atmosphere causes a million times lower global warming effect than that can be caused by SPVC solar panels.

CONCLUSIONS

The following conclusions can be made from the above study:

A device can be fabricated to experimentally measure the heat causing effect of commercially available SPV cells.

The SPV cells when employed in conjunction with γ -butyrolactone NWF to absorb the sunlight in a device generate more than 46°C top surface glass temperature when the room temperature is around 32 to 34°C. This about 14°C is a considerably high temperature when it is continuously released in to the atmosphere for more than about 5 hours period in a day from several square kilometers area. It will certainly cause a great global warming effect. This is the main reason for most of the unprecedented and un-controllable rains and floods occurring these days across the globe, for example, those recently occurred in Vijayawada city and Kerala state of India, and those in China, Dubai, and USA. Henceforth, all over the world the unprecedented and uncontrollable floods will continuously occur every year, which cannot be handled by no government across the globe unless all the SPVC solar panels are completely banned, or captured the heat energy generated by them to use for the beneficial purposes of the society, or completely replaced by the safe SLAPE solar panels after completely developing these latter safe solar panels.

The careful analysis of the experimental results of this study and the so far reported literature clearly indicates that the SPVC solar panels cause a million times higher global warming than the equivalent CO₂ gas present in the atmosphere, and the one generated upon burning fossil fuels to generate that much electricity can cause.

Nevertheless, further studies are required to precisely measure the actual amounts of heat energy generating abilities of SPV cells.

REFERENCES

1. Bockris, J. O. M. (2008) Hydrogen no longer a high cost solution to global warming: New ideas, *Int. J. Hydrogen Energy* 33, 2129-2131.
2. Couce, E., Ridgwell, A., and Hendy, E. J. (2013) Future habitat suitability for coral reef ecosystems under global warming and ocean acidification, *Global Change Biology* 19, 3592-3606.
3. de_Richter, R., and Caillol, S. (2011) Fighting global warming: The potential of photocatalysis against CO₂, CH₄, N₂O, CFCs, tropospheric O₃, BC and other major contributors to climate change, *Journal of Photochemistry and Photobiology C: Photochemistry Reviews* 12, 1-19.
4. Enzler, S. M. (2022) History of the greenhouse effect and global warming, <https://www.lenntech.com/greenhouse-effect/global-warming-history.htm#ixzz7Xxmlf434> <https://history.aip.org/climate/co2.htm>.
5. Ming, T., de_Richter, R., Liu, W., and Caillol, S. (2014) Fighting global warming by climate engineering: Is the Earth radiation management and the solar radiation management any option for fighting climate change?, *Renewable and Sustainable Energy Reviews* 31, 792-834.
6. Ganesh, I. (2024) Reason for India Not Producing a Single Nobel Laureate in Science Category during the Past 93 Years – A Scientist's Interpretation, *Pakistan Journal of Life and Social Sciences* 22, 4740-4747.
7. Ganesh, I. (2024) SLAPE solar panels: a possible solution for the future energy problems of our society, *Discover Sustainability* 5, 179.
8. Ganesh, I. (2024) A device and method for converting sunlight into heat energy using semiconducting materials immersed in a stable organic solvent for electricity generation, *Indian Patent* 517962 April
9. Ganesh, I. (2023) Semiconductor and Liquid Assisted Photothermal Effect: A New Method to Generate Electricity from Sunlight, *Preprints* 2023110965. <https://doi.org/10.20944/preprints202311.0965.v1>, 35.
10. Ganesh, I. (2023) EPDM rubber-based membranes for electrochemical water splitting and carbon dioxide reduction reactions, *Journal of Solid State Electrochemistry*; <https://doi.org/10.1007/s10008-023-05479-w>.

11. Ganesh, I. (2023) Practicable Artificial Photosynthesis: The Only Option Available Today for Humankind to Make Energy, Environment, Economy and Life Sustainable on Earth, *Book published by White Falcon Publishers ISBN Number 978-1-63640-828-6*, 1-716.
12. Ganesh, I. (2019) BMIM-BF₄ Mediated Electrochemical CO₂ Reduction to CO Is a Reverse Reaction of CO Oxidation in Air—Experimental Evidence, *The Journal of Physical Chemistry C* 123, 30198-30212.
13. Ganesh, I. (2018) The Electrochemical Conversion of Carbon Dioxide to Carbon Monoxide Over Nanomaterial Based Cathodic Systems: Measures to Take to Apply This Laboratory Process Industrially, Chapter 4 In *Applications of Nanomaterials* (Mohan Bhagyaraj, S., Oluwafemi, O. S., Kalarikkal, N., and Thomas, S., Eds.), pp 83-131, Woodhead Publishing.
14. Ganesh, I. (2016) Electrochemical conversion of carbon dioxide into renewable fuel chemicals – The role of nanomaterials and the commercialization, *Renewable and Sustainable Energy Reviews* 59, 1269-1297.
15. Ganesh, I. (2015) Solar fuels vis-a'-vis electricity generation from sunlight: The current state-of-the-art (a review), *Renewable Sustainable Energy Rev.* 44, 904-932.
16. Ganesh, I. (2014) Conversion of carbon dioxide into methanol – a potential liquid fuel: Fundamental challenges and opportunities (a review), *Renewable and Sustainable Energy Reviews* 31, 221-257.
17. Moore, F. C., and Diaz, D. B. (2015) Temperature impacts on economic growth warrant stringent mitigation policy, *Nature Climate Change* 5, 127-131.
18. Barber, J. (2007) Biological solar energy, *Philos Transact A Math Phys Eng Sci* 365, 1007-1023.
19. Barber, J. (2008) Crystal Structure of the Oxygen-Evolving Complex of Photosystem II, *Inorganic Chemistry* 47, 1700-1710.
20. Barber, M., Sharpe, P. K., and Vickerman, J. C. (1976) Studies of the surface behavior of oxide catalysts by secondary ion mass spectrometry (SIMS). 1. The surface composition of copper-containing spinel catalysts and their precursors, *Journal of Catalysis* 41, 240-248.
21. Blankenship, R. E., Tiede, D. M., Barber, J., Brudvig, G. W., Fleming, G., Ghirardi, M., Gunner, M. R., Junge, W., Kramer, D. M., Melis, A., Moore, T. A., Moser, C. C., Nocera, D. G., Nozik, A. J., Ort, D. R., Parson, W. W., Prince, R. C., and Sayre, R. T. (2011) Comparing photosynthetic and photovoltaic efficiencies and recognizing the potential for improvement, *Science* 332, 805-809.
22. J. Barber. (2003) Photosystem II: the engine of life. , *Q. Rev. Biophys* (doi:10.1017/S0033583502003839) 36, 71-89.
23. J. Barber. (2006) Photosystem II: an enzyme of global significance. (doi:10.1042/BST0340619), *Biochem. Soc. Trans.* 34, , 619-631.
24. J. Barber, K. Ferreira, K. Maghlaoui, and Iwata, S. (2004) Structure of the oxygen evolving center of photosystem II and its mechanistic implications. (doi:10.1039/b407981g), *Phys. Chem. Chem. Phys.* 6, 4737-4742.
25. Muradov, N. Z., and Veziroglu, T. N. (2008) "Green" path from fossil-based to hydrogen economy: An overview of carbon-neutral technologies, *Int. J. Hydrogen Energy* 33, 6804-6839.
26. Olah, G. A. (2005) Beyond oil and gas: The methanol economy, *Angew. Chem., Int. Ed.* 44, 2636-2639.
27. Barron-Gafford, G. A., Minor, R. L., Allen, N. A., Cronin, A. D., Brooks, A. E., and Pavao-Zuckerman, M. A. (2016) The photovoltaic heat island effect: Larger solar power plants increase local temperatures, *Scientific Reports* 6.
28. Du, D., Darkwa, J., and Kokogiannakis, G. (2013) Thermal management systems for Photovoltaics (PV) installations: A critical review, *Solar Energy* 97, 238-254.
29. Dupeyrat, P., Ménézo, C., Rommel, M., and Henning, H.-M. (2011) Efficient single glazed flat plate photovoltaic-thermal hybrid collector for domestic hot water system, *Solar Energy* 85, 1457-1468.

30. E.J. Brown, P.F. Baldasaro, S.R. Burger, L.R. Danielson, D.M. DePoy, G.J. Nichols, and Topper, W. F. (2003) The Status of Thermophotovoltaic Energy Conversion Technology at Lockheed Martin Corporation, *presented at Space Technology and Applications International Forum (STAIF), Albuquerque, N.M. (Feb. 2-5, 2003)*.
31. Eicker, U., and Dalibard, A. (2011) Photovoltaic-thermal collectors for night radiative cooling of buildings, *Solar Energy* 85, 1322-1335.
32. He, W., Chow, T. T., Ji, J., Lu, J., Pei, G., and Chan, L. S. (2006) Hybrid photovoltaic and thermal solar-collector designed for natural circulation of water, *Applied Energy* 83, 199-210.
33. Nelson, R. E. (2003) A Brief History of Thermophotovoltaic Development *Semiconductor Sci. Technol.* 18, S141-S143.
34. Panda, S., Gupta, M., Panda, B., Jena, C., Nanda, L., Pradhan, A., and Malvi, C. S. (2022) A review on advanced cooling techniques for photovoltaic panel, *Materials Today: Proceedings*.
35. Prakash, J. (1994) Transient analysis of a photovoltaic-thermal solar collector for co-generation of electricity and hot air/water, *Energy Conversion and Management* 35, 967-972.
36. Wang, N., Han, L., He, H., Park, N.-H., and Koumoto, K. (2011) A novel high-performance photovoltaic-thermoelectric hybrid device, *Energy & Environmental Science* 4, 3676.
37. S. Khandelwal, K. S. R., S. Srinivasa Murthy. (2007) Performance of contact and non-contact type hybrid photovoltaic-thermal (PV-T) collectors, *International Journal of Low-Carbon Technologies* 2, 359-375.
38. Mellor, A., Alonso Alvarez, D., Guarracino, I., Ramos, A., Riverola Lacasta, A., Ferre Llin, L., Murrell, A. J., Paul, D. J., Chemisana, D., Markides, C. N., and Ekins-Daukes, N. J. (2018) Roadmap for the next-generation of hybrid photovoltaic-thermal solar energy collectors, *Solar Energy* 174, 386-398.
39. Magalhães, P. M. L. P., Martins, J. F. A., and Joyce, A. L. M. (2016) Comparative Analysis of Overheating Prevention and Stagnation Handling Measures for Photovoltaic-thermal (PV-T) Systems, *Energy Procedia* 91, 346-355.
40. Parida, B., Iniyar, S., and Goic, R. (2011) A review of solar photovoltaic technologies, *Renewable and Sustainable Energy Reviews* 15, 1625-1636.

Video Captions

Video 1. Video showing the boiling of dichloromethane working fluid by absorbing the heat energy generated by SPV cells and γ -butyrolactone together out of the absorbed sunlight in a device.

Video 2. Video showing the generation of 16 V electricity by the heat energy generated by 21 numbers of commercially available multi-crystalline SPV cells in conjunction with 2 liters of γ -butyrolactone that was captured by dichloromethane working fluid and converted into rotational mechanical energy with the help of a reciprocally moved steam engine, and eventually electricity with the help of a custom-made electric generator containing four super strong magnets.

Video 3. Video showing about 46°C temperature measured on the surface of a device containing 21 numbers of commercially available multi-crystalline SPV cells and 2 liters of γ -butyrolactone upon exposure to sunlight having a power density of ~ 80 mW/cm² for 2 hours period at about 13:30 hours when the ambient room temperature was varied between 32°C and 34°C.

Table Captions

Table 1. Various limitations associated with silicon photovoltaic cell (SPVC) solar panels.

Table 2. The various reaction conditions and the values of sunlight-into-heat energy generated upon exposure of the device (100) with 21 numbers of SPV cells and different amounts of γ -butyrolactone NWF to the natural sunlight.‡

Table 3. The specific heat capacity and weights of various materials employed in the fabrication of device employed to measure the heat generating capability of silicon photovoltaic (SPV) cells.

Figure Captions

Fig. 1. A schematic diagram showing the various parts involved the fabrication of a device to measure the heat generating capability of silicon photovoltaic (SPV) cells.

Fig. 2. A digital photograph of the sunlight-to-heat energy generating device. Device was placed at an inclination of 30°; (a) front view, and (b) rear view.

Fig. 3. A schematic diagram showing the various parts involved and their associated operations in the generation of electricity from the heat energy generated by silicon photovoltaic (SPV) cells out of the absorbed sunlight using device.

Fig. 4. The volume of the device before (a) and after (b) exposing to the sunlight for more than 60 min when the 0.5 mm thick Al sheet has separated the top and bottom chambers and had 21 SPV cells immersed in 9.6 liters of γ -butyrolactone NWF. The average solar insolation was about 80 mW/cm² and the average room temperature was about 28°C.

Fig. 5. (a) Device with about 30 SPV cells with a packing factor of about 100% and about 2 liters γ -butyrolactone NWF and (b) the device connected to RMSE but not to the electric generator.

Fig. 6. Pressure readings in two-different pressure gauges with two different scales with up to 35 bar and up to 8 bar connected to the manifold of copper conduit tube containing about 1.8 liter dichloromethane WF of the device that was exposed to the sunlight between 9 am to 1 pm on 29th March 2022 (a) and on 28th March 2022 (b).

Table 1. Various limitations associated with silicon photovoltaic cell (SPVC) solar panels.

#	Limitation
1.	Theoretical efficiency of SPVCs is <30% (Shockley–Queisser limit)
2.	Sunlight absorption capacity is <70%
3.	Top solar glass reflects >10% incident sunlight
4.	Bas bar lines block up to 8% incident sunlight
5.	Generates only direct current electricity
6.	Maximum theoretical voltage generation with a single SPVC is <0.7 V
7.	Efficiency decreases with increasing operating temp. @ 0.5 V/°C
8.	Creates considerable local heat island effect
9.	They are neither repairable nor reusable
10.	It needs direct irradiation of sunlight unlike plant leaves need
11.	It contains toxic heavy metals like Pb
12.	Easily gets damaged when accidentally hit by a solid object
13.	It uses highly involved processes and equipment
14.	Uses highly toxic and pyrophoric chemicals to synthesize SPVCs
15.	When irradiated with 3 eV for example only 1.1 eV is converted into electricity and 1.9 eV is converted into heat energy only & Under open-circuit voltage (OCV) and short-circuit current (SCC) conditions, only heat energy is generated without any electricity
16.	Hence, theoretical efficiency of SPVC solar panels is <25%

Table 2. The various reaction conditions and the values of sunlight-into-heat energy generated upon exposure of the device (100) with 21 numbers of SPV cells and different amounts of γ -butyrolactone NWF to the natural sunlight.†

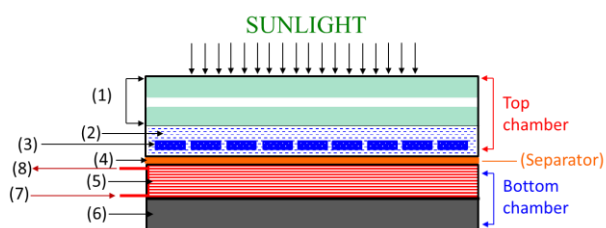
Light capturing system	γ -butyrolactone NWF (litres)	Metal that separates the top chamber from bottom chamber	Heat insulation given on top and bottom glasses (yes or no)	Temp. (°C) & pressure (bar) noted in WF) after 120 minutes of exposure to sunlight (± 2.0) [±]
SPV cells + γ -butyrolactone	2.3	Al (0.5 mm)	No	~54 & 0
SPV cells + γ -butyrolactone	10	Al (0.5 mm)	Yes	>40 & ~1.0
SPV cells + γ -butyrolactone	2.3	Al (0.5 mm)	Yes	>40 & >1.0
SPV cells + γ -butyrolactone	2.3	Cu (0.2 mm)	Yes	>40 & >1.5
SPV cells	0	Cu (0.2 mm)	Yes	>40 & <1.5
SPV cells + γ -butyrolactone	10	Cu (0.2 mm)	Yes	>40 & >3.0

†During some of the experiments, within two-hours of exposure to the sunlight, a lot of swelling of the device (100) at center portion was noted; if it was further exposed to the sunlight without opening the valve connected to the bottom chamber containing the DCM WF, the device would have been exploded since that kind of pressure generation and swelling of the device was noted.; [±]The

temperature and pressure values were measured using a thermometer and a pressure gauge, respectively.

Table 3. The specific heat capacity and weights of various materials employed in the fabrication of device employed to measure the heat generating capability of silicon photovoltaic (SPV) cells.

Material	Specific heat capacity (kJ/kg.°C)	Weight (grams)	Density (g/cm ³)
SPV cells	0.71	~11.9×21 = 249.9	2.33
Copper sheet (0.2 mm thick)	0.385	~1750	8.96
Aluminum sheet (0.5 mm thick)	0.90	~1020	2.70
γ-Butyrolactone NWF	1.642	~2576 (2.3 litres)	1.12
Dichloromethane WF	1.188	~2660 (2 litres)	1.33
Water	4.20	-	1.00



- (1) Flat glass vacuum chamber to transmit sunlight but to avoid heat loss as Dewar flask
- (2) γ-Butyrolactone to capture sunlight and turn it into heat energy (non-working fluid)
- (3) Silicon photovoltaic (SPV) cell (semiconductor)
- (4) 0.2 mm Cu sheet for high heat transfer from top chamber to WF in Cu tube conduit
- (5) Working fluid (WF) in Cu tube conduit present in bottom chamber
- (6) PUF thermal insulation to completely avoid heat loss from bottom chamber
- (7) Working fluid (WF) inlet
- (8) Working fluid (WF) vapor outlet with require pressure to rotate steam engine (ORC)

Fig. 1. A schematic diagram showing the various parts involved the fabrication of a device to measure the heat generating capability of silicon photovoltaic (SPV) cells.

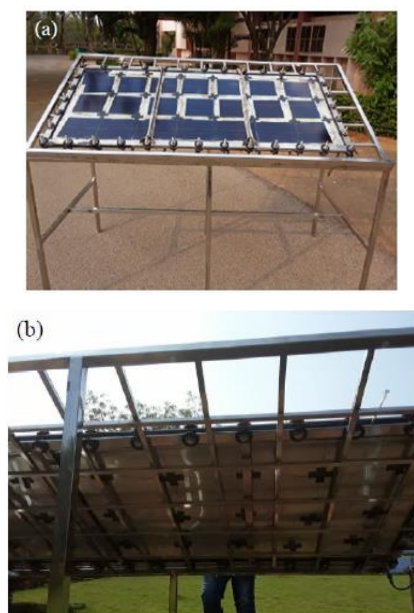


Fig. 2. A digital photograph of the sunlight-to-heat energy generating device. Device was placed at an inclination of 30°; (a) front view, and (b) rear view.

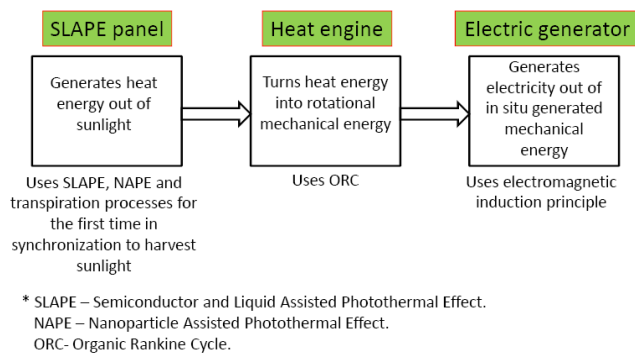


Fig. 3. A schematic diagram showing the various parts involved and their associated operations in the generation of electricity from the heat energy generated by silicon photovoltaic (SPV) cells out of the absorbed sunlight using



Fig. 4. The volume of the device before (a) and after (b) exposing to the sunlight for more than 60 min when the 0.5 mm thick Al sheet has separated the top and bottom chambers and had 21 SPV cells immersed in 9.6 litres of γ -butyrolactone NWF. The average solar insolation was about 80 mW/cm² and the average room temperature was about 28°C.



Fig. 5. (a) Device with about 30 SPV cells with a packing factor of about 100% and about 2 litres γ -butyrolactone NWF and (b) the device connected to RMSE but not to the electric generator.



Fig. 6. Pressure readings in two-different pressure gauges with two different scales with up to 35 bar and up to 8 bar connected to the manifold of copper conduit tube containing about 1.8 litre dichloromethane WF of the device that was exposed to the sunlight between 9 am to 1 pm on 29th March 2022 (a) and on 28th March 2022 (b).

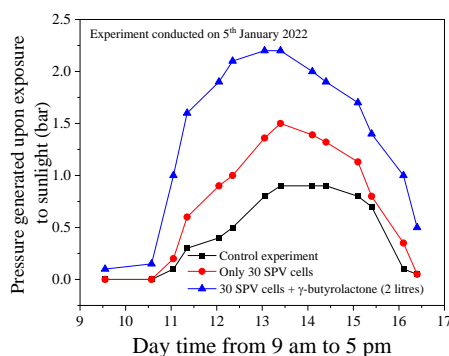


Fig. 7.

Appendix:

Supporting Information Figures Captions

Fig. S1. A schematic diagram showing an exploded view of device (100) employed to measure the heat generating capability of silicon photovoltaic (SPV) cells with partial hidden details.

Fig. S2. A schematic diagram showing a side view of device (100) employed to measure the heat generating capability of silicon photovoltaic (SPV) cells with partial hidden details.

Fig. S3. A schematic diagram showing the top view of device (100) employed to measure the heat generating capability of silicon photovoltaic (SPV) cells with partial hidden details.

Fig. S4. A schematic diagram showing the backside view of device (100) employed to measure the heat generating capability of silicon photovoltaic (SPV) cells with partial hidden details.

Fig. S5 A schematic diagram of the reciprocally moved steam engine (200) along with a digital photo of its lab-scale working model attached with a schematic diagram showing the partial details of an electric generator (300).

Fig. S6. A schematic diagram of an electric generator (300) with partial hidden details.

Fig. S7. The digital photographs of exploded device (100) (a), along with the swelled and bent images of SS 204 frames (a & c) and 1.1 mm thick copper sheet (1480 × 660 mm) (b & d).

Fig. S8. Copper tube (3/8th inch diameter) being brazed on a 1.1 mm thick copper sheet of 1480 mm length × 660 mm width to prepare copper conduit attached to copper sheet.

Fig. S9. (a) SLAPE solar panel containing about 30 silicon photovoltaic cells with a packing factor of about 100% and about 2 litres γ -butyrolactone solution; (b) SLAPE panel connected with reciprocally moved steam engine but not with electric generator; (c) the pressure gauge connected to the copper conduit manifold of the bottom chamber of SLAPE solar panel showing the value of 28 bar recorded on 30th March 2022 after exposing the panel for 2.5 hours duration (between 9 am and 12 pm); and (d) reciprocally moved steam engine connected with a direct current electric generator and 12 W LED bulb, which are connected to SLAPE solar panel's copper conduit.

Fig. S10. Digital photographs showing SLAPE solar panel with 30 silicon photovoltaic cells used for glowing the 5 W LED bulb (a), 5 W LED bulb glowing, reciprocally moved steam engine in action (c), around 46°C temperature measured for top solar glass of SLAPE panel with 30 SPV cells and room temperature of about 34°C (d), 16.70 V alternating current seen in a multi-meter generated by SLAPE solar panel containing 21 SPV solar cells (e), dichloromethane exhaust from reciprocally moved steam engine (f), and SLAPE solar panel with 21 solar

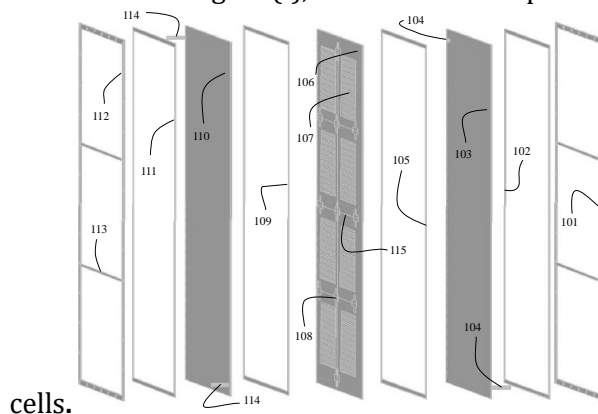


Fig. S1. A schematic diagram showing an exploded view of device (100) employed to measure the heat generating capability of silicon photovoltaic (SPV) cells with partial hidden details.

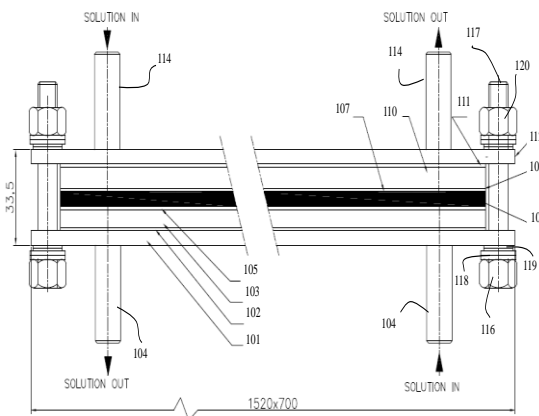


Fig. S2. A schematic diagram showing a side view of device (100) employed to measure the heat generating capability of silicon photovoltaic (SPV) cells with partial hidden details.

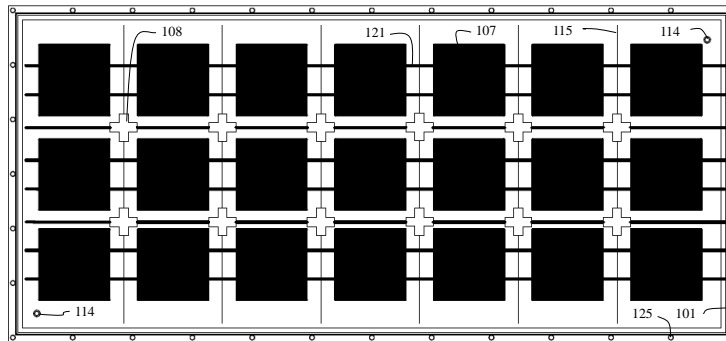


Fig. S3. A schematic diagram showing the top view of device (100) employed to measure the heat generating capability of silicon photovoltaic (SPV) cells with partial hidden details.

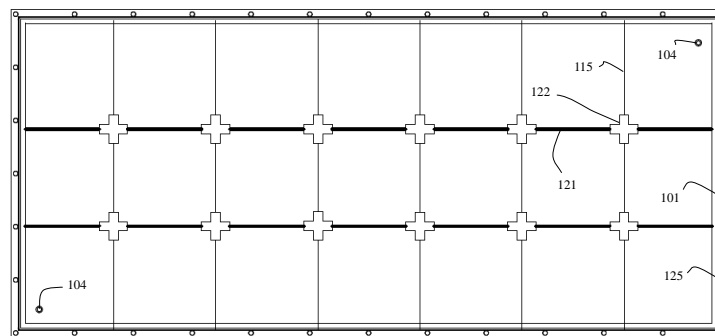


Fig. S4. A schematic diagram showing the backside view of device (100) employed to measure the heat generating capability of silicon photovoltaic (SPV) cells with partial hidden details.

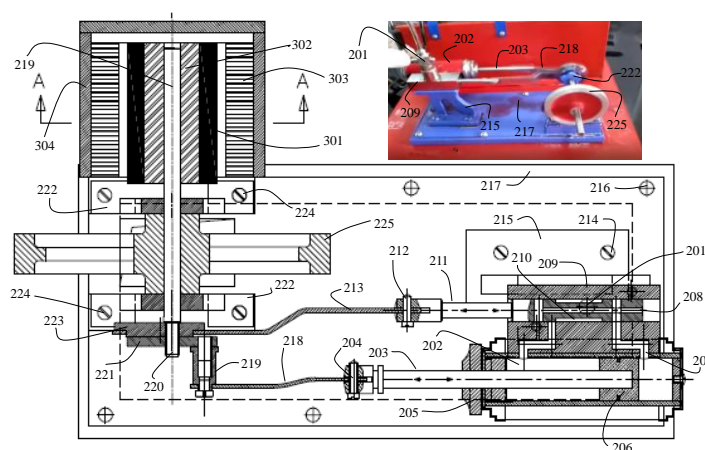


Fig. S5 A schematic diagram of the reciprocally moved steam engine (200) along with a digital photo of its lab-scale working model attached with a schematic diagram showing the partial details of an electric generator (300).

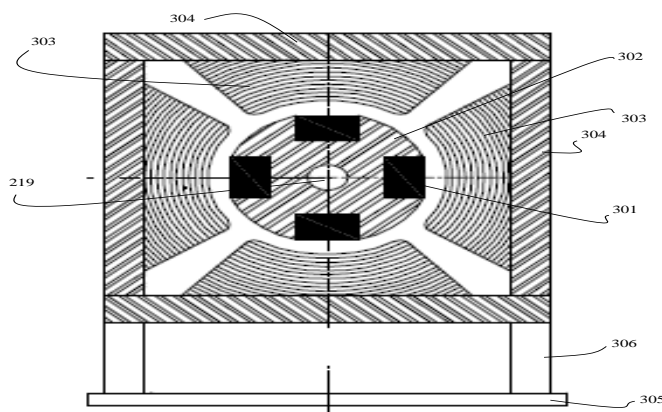


Fig. S6. A schematic diagram of an electric generator (300) with partial hidden details.

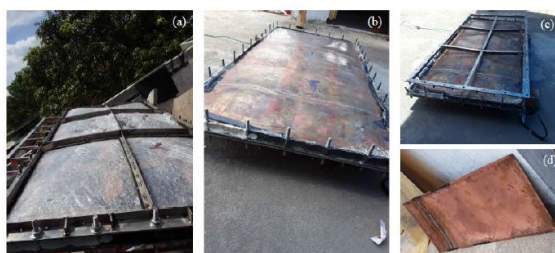


Fig. S7. The digital photographs of exploded device (100) (a), along with the swelled and bent images of SS 204 frames (a & c) and 1.1 mm thick copper sheet (1480 × 660 mm) (b & d).



Fig. S8. Copper tube (3/8th inch diameter) being brazed on a 1.1 mm thick copper sheet of 1480 mm length × 660 mm width to prepare copper conduit attached to copper sheet.



Fig. S9. (a) SLAPE solar panel containing about 30 silicon photovoltaic cells with a packing factor of about 100% and about 2 litres γ -butyrolactone solution; (b) SLAPE panel connected with reciprocally moved steam engine but not with electric generator; (c) the pressure gauge connected to the copper conduit manifold of the bottom chamber of SLAPE solar panel showing the value of 28 bar recorded on 30th March 2022 after exposing the panel for 2.5 hours duration (between 9 am and 12 pm); and (d) reciprocally moved steam engine connected with a direct current electric generator and 12 W LED bulb, which are connected to SLAPE solar panel’s copper conduit.

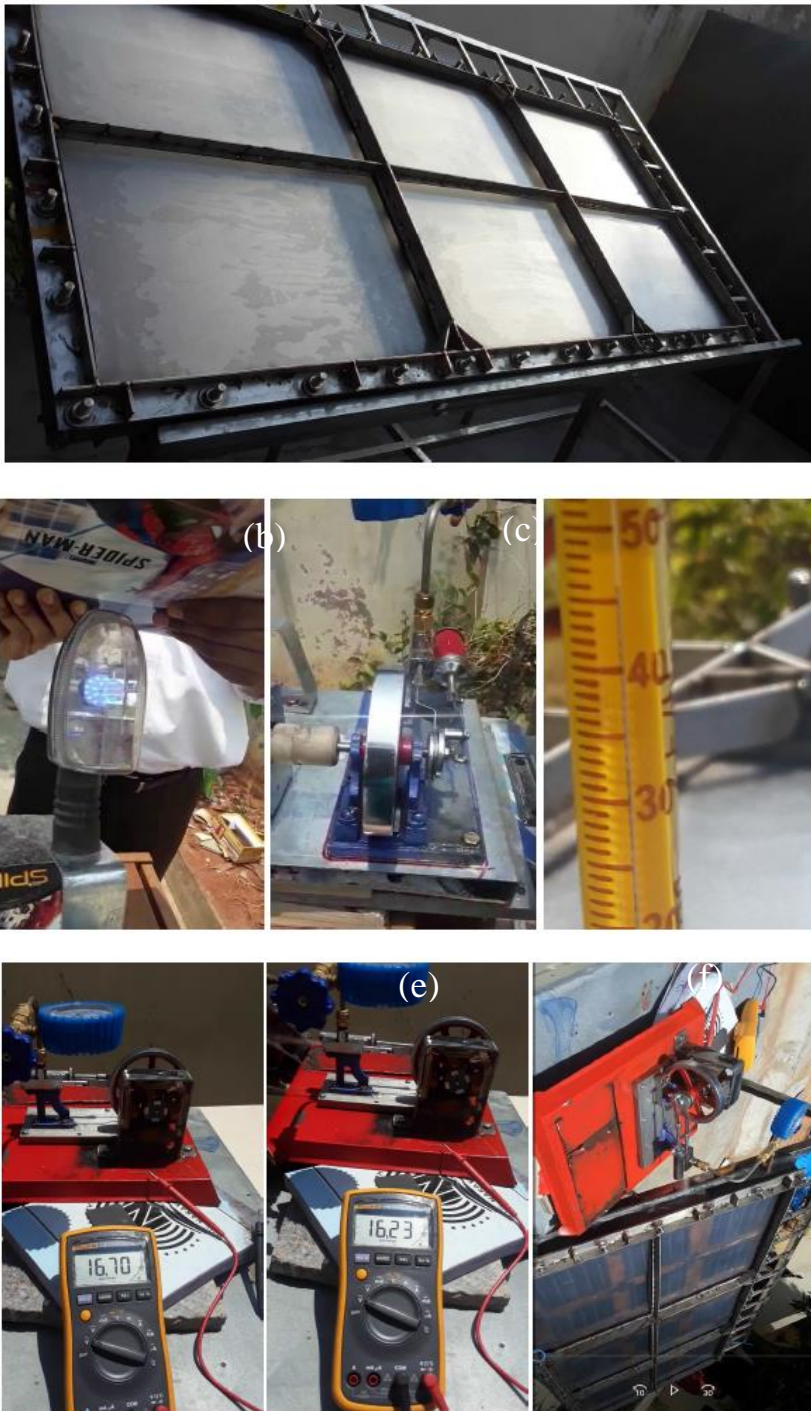


Fig. S10. Digital photographs showing SLAPE solar panel with 30 silicon photovoltaic cells used for glowing the 5 W LED bulb (a), 5 W LED bulb glowing, reciprocally moved steam engine in action (c), around 46°C temperature measured for top solar glass of SLAPE panel with 30 SPV cells and room temperature of about 34°C (d), 16.70 V alternating current seen in a multi-meter generated by SLAPE solar panel containing 21 SPV solar cells (e), dichloromethane exhaust from reciprocally moved steam engine (f), and SLAPE solar panel with 21 solar cells.